AIP | Journal of Applied Physics

Transport characteristics of AlGaN/GaN/AlGaN double heterostructures with high electron mobility

Fanna Meng, Jincheng Zhang, Hao Zhou, Juncai Ma, Junshuai Xue et al.

Citation: J. Appl. Phys. **112**, 023707 (2012); doi: 10.1063/1.4739408
View online: http://dx.doi.org/10.1063/1.4739408
View Table of Contents: http://jap.aip.org/resource/1/JAPIAU/v112/i2
Published by the American Institute of Physics.

Transport characteristics of AlGaN/GaN/AlGaN double heterostructures with high electron mobility

Fanna Meng,[a] Jincheng Zhang,[b] Hao Zhou, Juncai Ma, Junshuai Xue, Lisha Dang, Linxia Zhang, Ming Lu, Shan Ai, Xiaogang Li, and Yue Hao
Key Laboratory of Wide Band Gap Semiconductor Materials and Devices, School of Microelectronics, Xidian University, Xi'an 710071, People's Republic of China

(Received 24 March 2012; accepted 27 June 2012; published online 26 July 2012)

The AlGaN/GaN/AlGaN double heterostructure (DH) with high electron mobility of 1862 cm^2/Vs at room temperature and 478 cm^2/Vs at 573 K high temperature was obtained by a combination of optimization schemes considering scattering mechanisms. First, a composite buffer layer structure, including GaN and AlGaN layer, was used to improve the crystal quality of the AlGaN/GaN/AlGaN DH. Second, interface roughness scattering was reduced by increasing the channel thickness, thus the two-dimensional electron gas mobility was further improved. Moreover, an ultrathin AlN interlayer was inserted between the GaN channel layer and the AlGaN buffer layer to decrease the alloy disorder scattering. The Hall effect measurements showed that the DH had better transport characteristics at high temperatures, and an electron mobility of 478 cm^2/Vs was achieved at 573 K, which is twice larger than that of the conventional single heterostructure (~200 cm^2/Vs at 573 K). Therefore, AlGaN/GaN/AlGaN DH is more suitable for the applications in high temperature electronic devices. © *2012 American Institute of Physics*. [http://dx.doi.org/10.1063/1.4739408]

I. INTRODUCTION

GaN-based high electron mobility transistors (HEMTs) are considered to be promising for high-voltage, high-power, and high-temperature microwave applications due to the extraordinary physical properties.[1,2] During the past two decades, tremendous progresses have been achieved to ameliorate the material quality and device processing techniques, for example, improved growth method of pulsed metal organic chemical vapor deposition (MOCVD) and the introducing of field plate structures.[3–5] Meanwhile, numerical simulation as an efficient and economical way has being increasingly employed for exploring advanced device structures and their applications,[6–8] and many novel and advanced device structures are being proposed for further performance improvement. Among these proposed emerging structures, double-channel and composite-channel HEMTs have been studied for higher carrier density and improved linearity.[9–12] In addition, double heterojunction HEMTs are also being investigated to improve carrier confinement, which enables improvement of the device performance, i.e., lower leakage current and enhanced breakdown voltage. Double heterojunction HEMTs with an InGaN layer serving as the channel or the back-barrier have been proposed for better carrier confinement, but the low mobility and crystalline quality of the InGaN layer are the major hurdles.[13,14] In order to further improve the breakdown characteristics for high voltage applications, it is an attractive alternative to use AlGaN instead of GaN as the buffer layer, which is due to the wider energy band gap and higher breakdown fields of AlGaN. However, it is more difficult to obtain a high-quality AlGaN buffer layer than GaN buffer layer. Compared to the conventional AlGaN/GaN HEMT, the breakdown voltage of the fabricated AlGaN/GaN/AlGaN HEMT device was remarkably enhanced but the crystalline quality and two-dimensional electron gas (2DEG) transport properties of the material were degenerated, bringing detrimental effects to the DC device characteristics.[15–17]

In this paper, we explore and demonstrate several specific approaches for optimizing the AlGaN/GaN/AlGaN structure to improve the material characteristics, as well as improved device performance, taking into consideration the most relevant scatterings, including dislocation scattering, alloy disorder scattering, interface roughness scattering, polar optical phonon scattering, etc. First, a composite buffer structure with GaN and AlGaN is employed to improve the crystal quality and to reduce threading dislocation density of the AlGaN/GaN/AlGaN double heterostructure (DH), because dislocations in the buffer layer will extend upward in the subsequent growth process, and even penetrate the surface making a great impact on the crystal quality, surface morphology, and electrical properties of the materials, thereby deteriorating the device performances. Considering that 2DEG moves in the GaN channel layer, the GaN channel thickness is optimized to further improve the electron mobility. Due to AlGaN ternary alloy as the buffer layer, the impact of alloy disorder scattering on the 2DEG transport properties also exists beneath the channel layer, thus an ultrathin AlN interlayer is introduced between the GaN channel layer and the AlGaN buffer layer to depress alloy disorder scattering and further increase the 2DEG mobility.[18] The optimized AlGaN/GaN/AlGaN/GaN DH exhibits higher crystal quality and better transport properties. In addition, it is necessary to study the high-temperature electron transport

[a]Electronic mail: mengfna@163.com.
[b]Author to whom correspondence should be addressed. Electronic mail: jchzhang@xidian.edu.cn.

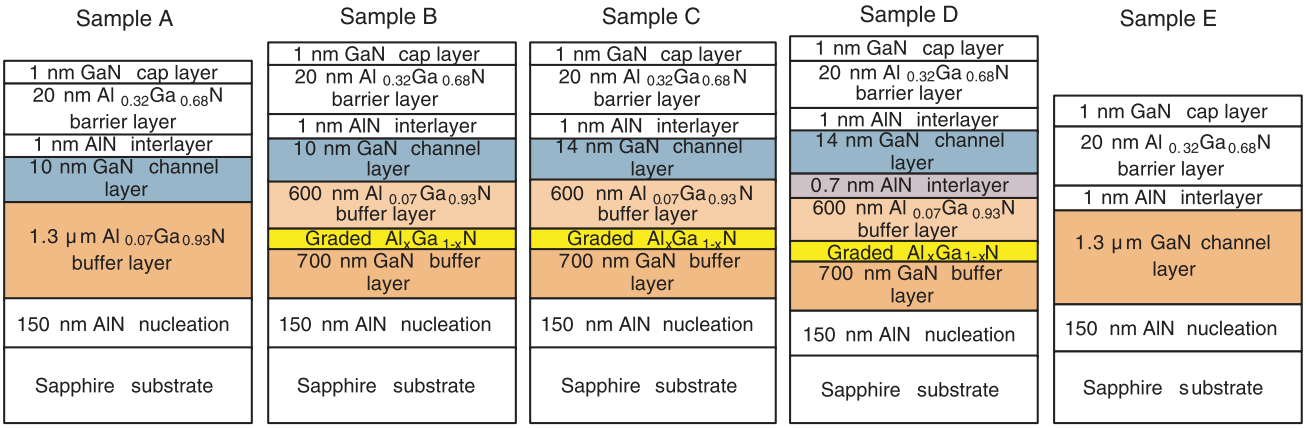

FIG. 1. Schematic cross sections of samples A-E.

characteristics of the heterostructure due to devices generally operating at 200 °C or even higher. Previous temperature dependence of electrons transport property study of GaN-based HEMTs mainly focused on the AlGaN/GaN single heterostructure (SH).[19,20] Here, we investigate the electron transport characteristics of DHs with the variable temperature from 77 K to 573 K by Hall effect using a van der Pauw configuration, which shows that DHs are more suitable for the applications in high temperature devices because of DHs' higher electron mobility and steadier carrier density than those of the conventional SH at elevated temperatures.

II. EXPERIMENTRAL PROCEDURE

All structures, with the schematic cross sections shown in Fig. 1, were grown by low pressure MOCVD on 2-in. *c*-plane sapphire substrates. Trimethylalumium (TMAl), triethylgallium (TEGa), and ammonia (NH_3) were used as the sources of Al, Ga, and N, respectively. Hydrogen was used as a carrier gas. All samples have the same AlN nucleation layer grown at 1050 °C after annealing the substrates in H_2 ambient for 10 min at 1050 °C. For a single AlGaN buffer structure (denoted sample A) and three composite AlGaN/GaN buffer structures (denoted samples B-D), a 1.3 μm $Al_{0.07}Ga_{0.93}N$ and a 700 nm GaN followed by a 600 nm $Al_{0.07}Ga_{0.93}N$ buffer layer were grown, respectively. In order to avoid the generation of a minor channel in the buffer layer, a linearly graded $Al_xGa_{1-x}N$ ($x = 0 \sim 0.07$) layer at the interface of AlGaN and GaN buffer layer was done. Then only sample D had a 0.7 nm AlN interlayer after growing the $Al_{0.07}Ga_{0.93}N$ buffer layer. Subsequently, an unintentionally doped GaN channel layer was grown followed by a 1 nm AlN interlayer. Finally, a 20 nm top $Al_{0.32}Ga_{0.68}N$ barrier layer and a 1 nm GaN cap layer were deposited. For comparison, a conventional SH (sample E) was grown using a 1.3 μm GaN buffer layer instead of the AlGaN buffer layer of sample A, and the other layers were grown in the same conditions as that in DH. By self-consistently solving the one-dimensional Poisson-Schrödinger equation, the conduction band diagrams of samples D and E are presented in Fig. 2(a). The energy levels and wavefunctions of electrons are shown in Fig. 2(b), which indicates that the 2DEG confinement is improved in sample D.

The crystal quality and surface morphology of the samples were characterized by high resolution x-ray diffraction (HRXRD) and atomic force microscope (AFM), respectively. Additionally, the 2DEG mobility at room temperature was performed by the noncontact Hall measurement (LEI-1610E100M). To characterize the temperature dependence of the 2DEG transport properties, the Hall effect measurement

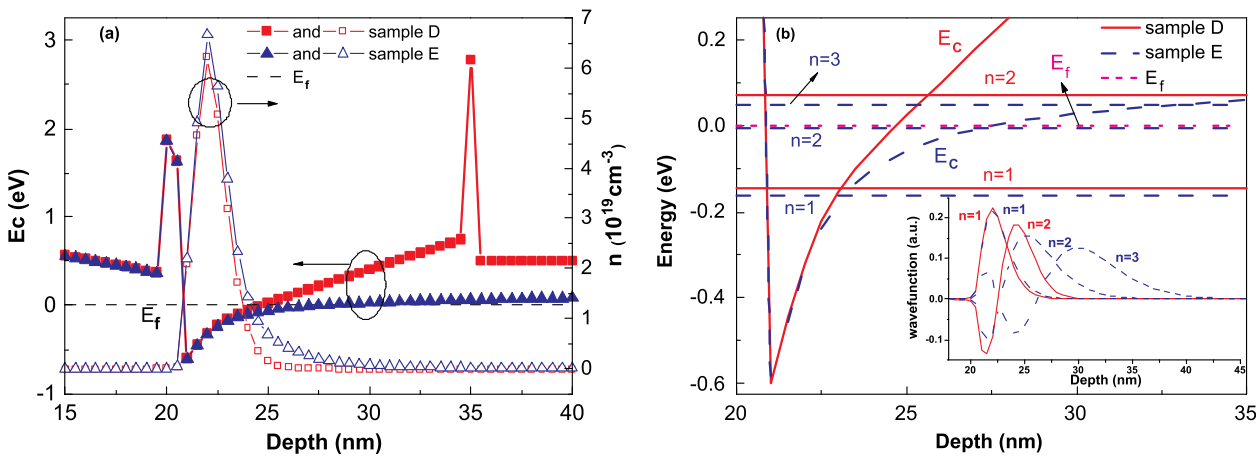

FIG. 2. Calculated (a) conduction band diagrams and electron distributions and (b) the energy levels and wavefunctions of electrons for samples D and E at room temperature. For sample E, the first three subbands energy levels and wavefunctions were given in the figure. n = 1, 2, 3.

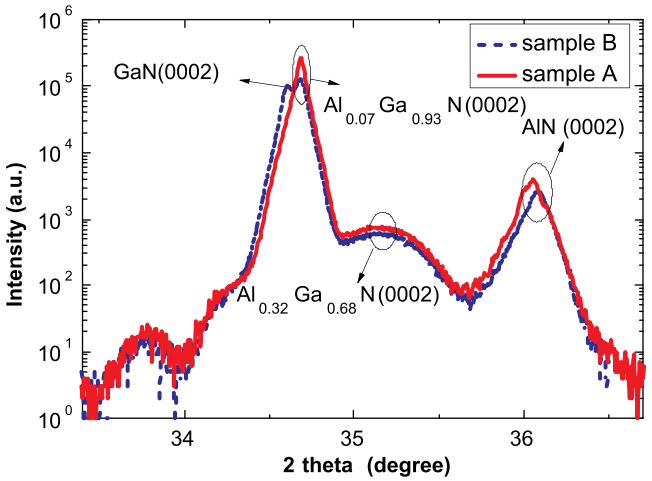

FIG. 3. High resolution XRD (0002) 2θ-ω scans of samples A and B.

was carried out by the van der Pauw technique in the temperature range from 77 K to 573 K using an Accent HL5500 Hall effect measurement system.

III. RESULTS AND DISCUSSION

It is believed that the insertion of an AlN interlayer and the variation of channel thickness could hardly affect the crystal quality, so only XRD and AFM results of sample A and sample B are presented here. Figure 3 shows the (0002) XRD 2θ-ω scans of samples A and B. Both structures have approximately the same peak position of the $Al_{0.32}Ga_{0.68}N$ barrier layer and AlN nucleation layer. However, there is only an $Al_{0.07}Ga_{0.93}N$ buffer layer peak at an angle of about 34.685° in sample A, while there are a GaN buffer layer peak at 34.605° and an $Al_{0.07}Ga_{0.93}N$ buffer layer peak at 34.685° in sample B. To evaluate the crystalline quality, the x-ray rocking curves for (0002) and (10-12) diffractions of buffer layers of heterostructures were measured by HRXRD. Figure 4 clearly shows the (0002) and (10-12) ω-scan rocking curves which were obtained through normalized angle and intensity in order to contrast and to determine the full widths at half maximum (FWHMs) of rocking curves. The (0002) FWHMs of GaN buffer layer and $Al_{0.07}Ga_{0.93}N$ buffer layer for sample B are 158 arc sec and 165 arc sec, respectively, larger than the 102 arc sec of $Al_{0.07}Ga_{0.93}N$ buffer layers for sample A, as shown in Fig. 4(a). However, as can be seen from Fig. 4(b), the (10-12) FWHMs of samples A and B are 835 arc sec and 492 arc sec, respectively. Rocking curve FWHMs depend on the dislocation density, in which screw dislocations affect the FWHMs of rocking curves for (0002) peak and edge dislocations affect those for (10-12) peak.[21] The edge dislocation density can be expressed as

$$D_B = \frac{\beta^2}{4.35b^2}, \quad (1)$$

where D_B is the edge dislocation density, β is the ω-FWHM, and b is the length of the Burgers vector. The edge dislocation density of sample B is decreased greatly by employing the composite buffer layer. For comparison, the reduction of edge dislocations is essential for the increase of 2DEG mobility, which will be shown in the following paragraphs.

Figure 5 shows the typical AFM images with $5 \times 5\ \mu m^2$ scan area of the surfaces of the epitaxial layers for sample A and sample B. Fine atomic steps and some small pits which correspond to dislocations can be clearly seen on both samples. However, there are a lot of V-pits generated by dislocations and roll of steps deteriorating the surface of AlGaN/GaN/AlGaN DH (sample A). The surface roughness in terms of root mean square (RMS) and surface relief height were measured to be 0.286 nm and 4.042 nm, respectively. Correspondingly, the RMS value and surface relief height of sample B were as low as 0.218 nm and 2.571 nm, respectively, which indicate the relatively smoother surface.

It can be clearly observed that the improvement of the material quality and the reduction of surface roughness are expected by using the composite structure of GaN and AlGaN buffer layer. In particular, the material quality and surface morphology are related to the adatom diffusion on the growing surfaces.[22] Compared to Ga atoms, Al atoms are easily "trapped" at sites that not correspond to the ideal lattice positions due to the low adatom diffusion, leading to the difficulty of obtaining high-quality and smooth AlGaN epilayer. As the thickness of AlGaN film increases, it results in

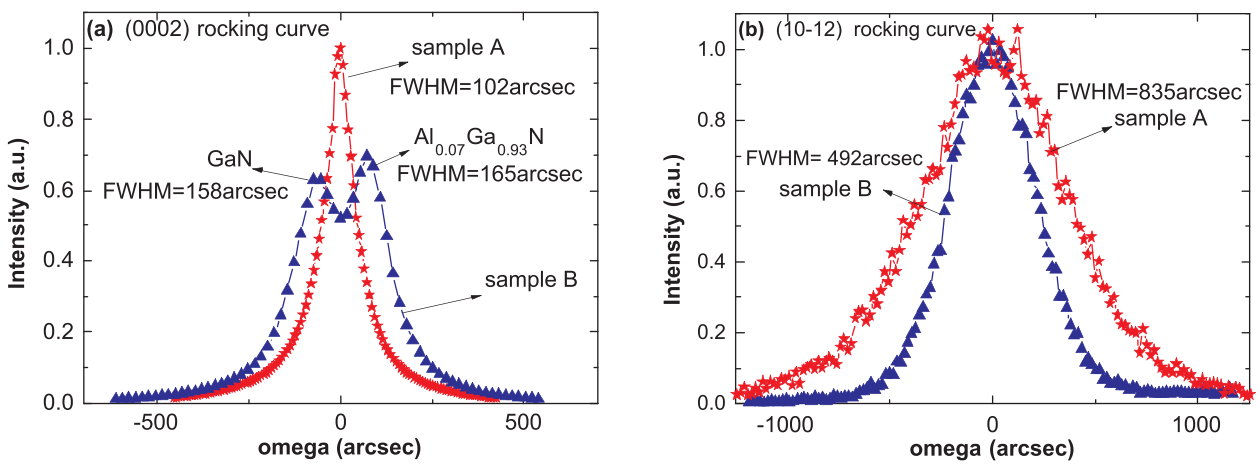

FIG. 4. XRD (a) (0002) and (b) (10-12) ω-scan rocking curves of samples A and B.

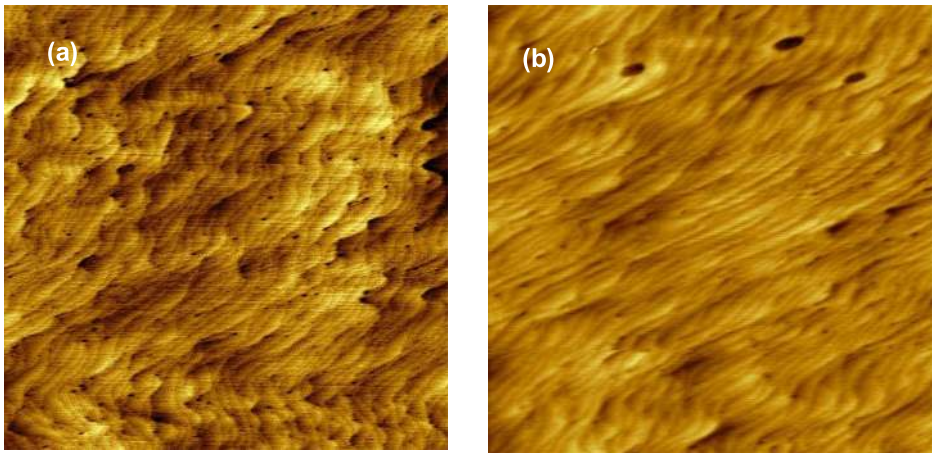

FIG. 5. AFM images of the surfaces of (a) sample A and (b) sample B. The imaged area is $5 \times 5\ \mu m^2$.

material surface fluctuation and quality deterioration, even creaks. Contrarily, the Ga adatoms are highly mobile and a step-flow growth mode resulting in 2D growth is expected. As thickness increases, the crystalline quality of GaN epilayer is improved with a flat surface due to parts of the dislocations mergence and annihilation along the growth front, while the quality is little improved when the thickness is exceeding 600 nm.[23] Owing to low lattice mismatch, 600 nm high-quality AlGaN with low Al component can be easier grown on 700 nm high-quality GaN buffer layer relatively. In addition, capacitance-voltage (*C-V*) measurement for sample D was carried out to profile the carrier distribution. The result shows that no minor channel was formed in the interface of AlGaN/GaN buffer layer (as shown in Fig. 6) due to the insertion of a graded $Al_xGa_{1-x}N$ layer between $Al_{0.07}Ga_{0.93}N$ and GaN buffer layer (as shown in Fig. 1).

The electrical properties of four samples at room temperature from the noncontact Hall measurements are shown in Table I. The hall mobilities of samples A-D were gradually improved by gradually optimizing the heterostructures. Owing to the low edge dislocations related to the GaN/AlGaN buffer layer, sample B exhibited a 2DEG mobility of 1752 cm^2/Vs and sheet carrier density of $1.06 \times 10^{13}\ cm^{-2}$ at room temperature, which are larger than those of sample A.

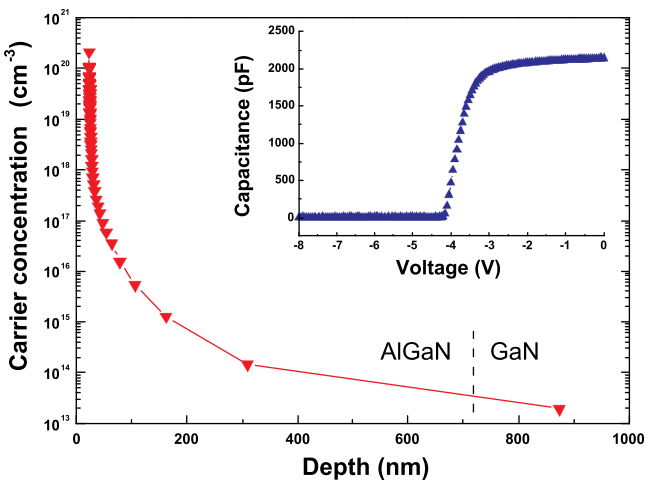

FIG. 6. Depth profile of carrier concentration extracted from the measured *C-V* curve (the inset diagram).

For sample C, increasing the channel thickness also improves the electron mobility due to the reduced interface roughness scattering, which has a major impact on semiconductor heterostructures especially in narrower wells. Due to the employment of AlGaN buffer layer with disordered distribution of Ga atoms and Al atoms, there exits alloy disorder scattering in the GaN/AlGaN interface beneath the channel. After absorbing an AlN interlayer between the channel layer and buffer layer, the alloy disorder scattering acting on the 2DEG will be reduced, which improves the electron mobility, despite the increment of mobility, as shown in Table I, is not so larger relatively by reasons of more 2DEG distributing on the top surface of the channel and the AlGaN buffer layer with lower Al composition. We consider that a larger increment of 2DEG mobility will be observed if the AlN interlayer is introduced into narrower channel double heterojunction or the AlGaN alloy buffer with an Al composition from 10% to 90% due to the alloy scatting of phonons.[24] Additionally, the AlN interlayer beneath the channel will increase the carrier confinement.

To further investigate the 2DEG electrical properties, temperature-dependent Hall measurements of the conventional SH and four DH materials were carried out from 77 K to 573 K using a van der Pauw configuration. Figure 7 shows the temperature dependencies of the mobility and sheet carrier density in the conventional SH and DHs. The Hall mobilities of all the samples gradually decrease as the temperature increases, and that their decrease ratios decrease with increasing the temperature, as shown in Fig. 7(a).

The low-temperature mobility is mostly limited by alloy disorder and interface roughness scattering mechanisms.[25–27]

TABLE I. The electrical properties obtained by noncontact Hall measurements at room temperature, (10-12) FWHMs and RMS for four samples.

	Sample A	Sample B	Sample C	Sample D
Carrier mobility (cm^2/Vs)	1508	1752	1821	1862
Sheet carrier density ($10^{13}\ cm^{-2}$)	0.85	1.06	1.04	0.95
Sheet resistance (Ω/sq)	450	354	340	362
(10-12) FWHM (arc sec)	835	492	481	512
RMS (nm)	0.286	0.218	0.225	0.221

Kearley and Horrell gave the mobility expression of alloy disorder scattering without screening effects as[28]

$$\mu_{\text{alloy}} = \frac{16}{3b}\frac{e\hbar^3}{x(1-x)m^{*2}\Omega_0 U_{AL}^2}, \tag{2}$$

where x is the alloy mole fraction, Ω_0 is the volume occupied by one atom, and U_{AL} is the alloy potential. The mobility of interface roughness scattering is given by[25]

$$\mu_{IFR} = \left(\frac{2\varepsilon_0\varepsilon_s}{n_{2D}\Delta\Lambda}\right)^2 \frac{\hbar^3}{e^3 m^{*2}}\frac{1}{J_{IFR}(k)}, \tag{3}$$

where Δ is the lateral size of the roughness and Λ is the correlation length between fluctuations. The integral $J_{IFR}(k)$ in Eq. (3) is defined as

$$J_{IFR}(k) = \int_0^{2k} \frac{e^{-q^2\Lambda^2/4}}{2k^3(q+q_s)^2\sqrt{1+(q/2k)^2}} q^4 dq, \tag{4}$$

where q_s is the screening constant. There is only one interface between the barrier layer and channel layer in the conventional SH, but for the DH there exists a second interface beneath the channel owing to employing the AlGaN buffer layer. The unique channel-buffer interface and larger interface roughness in DH lead to larger alloy disorder scattering and interface roughness scattering, therefore, the hall mobility of conventional SH sample is higher than that of DH samples at low temperatures. However, through the three optimization schemes, the two kinds of carrier scattering are weakened and the hall mobility of sample D is dramatically improved to be 5797 cm^2/Vs at 77 K, which approaches the value of the conventional SH (5973 cm^2/Vs at 77 K).

At high temperatures, the polar optical phonon scattering is the dominant mechanism, and the effects of interface roughness and alloy disorder scattering mechanisms only have a negligible impact on the mobility.[26,27] The expression of the mobility limited by the polar optical phonon scattering is given by Ridley as[29]

$$\mu_{po} = \frac{4\pi\varepsilon_0\varepsilon_p\hbar^2}{e\omega m^{*2}Z_0}[e^{\hbar\omega/k_BT} - 1], \tag{5}$$

where

$$\frac{1}{\varepsilon_p} = \frac{1}{\varepsilon_\infty} - \frac{1}{\varepsilon_s}. \tag{6}$$

Here, $\hbar\omega$ is the polar optical phonon energy, ε_∞ and ε_s are the high and low frequency dielectric constants, respectively. m^* is the effective mass. Moreover, the hall mobility is the comprehensive effect of two-dimensional electrons and bulk electrons. The measured carrier density and mobility can be expressed as[30]

$$n_M\mu_M = n_{2DEG}\mu_{2DEG} + n_{buf}\mu_{buf}, \tag{7}$$

by using the Hall effect model, where n_M and μ_M represent the measured sheet 2DEG density and mobility, n_{2DEG} and μ_{2DEG} are the actual sheet 2DEG density and mobility and n_{buf} and μ_{buf} are the sheet electron concentration and mobility of bulk electrons in the underlying GaN or AlGaN buffer layer. Compared to the mobility of two-dimensional electrons, the mobility of bulk electrons moving in a three-dimensional way is lower. At high temperatures, shallow donor impurities in the GaN or AlGaN buffer layer ionize and then promote background carrier density. Meanwhile, as the temperature increases, parts of the channel electrons acquiring sufficient energy can spill over from the potential well and become three-dimensional electrons with low mobility, which has a severe influence upon the hall mobility of the whole material system. However, in the DHs, the increased back-barrier height of AlGaN buffer layer suppresses the 2DEG spillover into buffer layer, especially at high temperatures. As shown in the Fig. 7(a), the electron mobility of the DH (sample D) determined to be 478 cm^2/Vs at 573 K, which is significantly higher than that of the conventional SH around 200 cm^2/Vs. Wang *et al.* have achieved a 2DEG mobility of about 210 cm^2/Vs at 573 K for the conventional SH, which is also much lower than our result.[20] It can be confirmed that the DH reveals better high-temperature electron transport characteristics.

Figure 7(b) shows the sheet carrier density of samples as a function of temperature. The sheet carrier density of the conventional SH sample decreases with increasing the

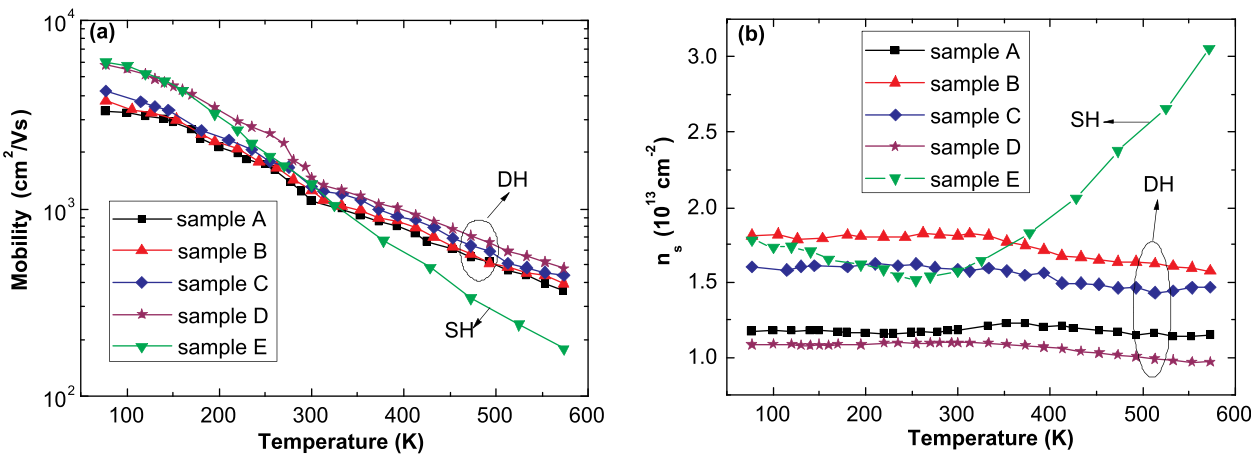

FIG. 7. (a) The hall mobility and (b) sheet carrier density for each sample as a function of temperature.

temperature from 77 K to 250 K, but afterwards it increases with increasing the temperature. It is suggested that the negative coefficient of the sheet carrier density in low temperature range is caused by the reduction of the conduction band offset, and the positive coefficient of that at high temperatures is attributed to the increased background electron concentration in the buffer layer.[20] For the DH materials, high-barrier and high-resistance AlGaN buffer layer not only effectively suppresses the channel carriers overflow the buffer layer but also displays an excellent isolation behavior. Therefore, it can be observed that the carrier densities in the four DH samples show very little variation with the temperature up to 573 K, which demonstrates very good carrier confinement and high-quality of the materials. Based on the analysis above, it can be concluded that better electron transport characteristic was realized from the AlGaN/GaN/AlGaN/GaN heterostructures at high temperatures and the DH devices have lower leakage current and higher breakdown voltage than the conventional SH devices do.

IV. CONCLUSIONS

Four gradually varied AlGaN/GaN/AlGaN DHs and a conventional SH were grown by MOCVD on sapphire substrates. We have successfully achieved an AlGaN/GaN/AlGaN/GaN DH with high 2DEG mobility of 1862 cm^2/Vs at room-temperature and 478 cm^2/Vs at 573 K by using an optimization scheme which contains adopting the composite buffer layer, increasing the channel thickness and introducing the ultrathin AlN interlayer between the GaN channel layer and AlGaN buffer layer to improve the crystal quality and decrease the interface roughness scattering and alloy disorder scattering, respectively. Temperature dependencies of Hall mobility and sheet carrier density in the conventional SH and four DHs have been compared and investigated by temperature Hall measurements ranging from 77 K to 573 K. It is illustrated that DHs have better transport characteristics at high temperatures, and electron mobility of sample D determined to be 478 cm^2/Vs at 573 K, which is double times larger than that of the conventional SH ($\sim$200 cm^2/Vs at 573 K). The structural and electrical characterizations presented above imply that the AlGaN/GaN/AlGaN/GaN DH-HEMT can achieve much higher transconductance and gain. In addition, it is a promising structure for high-voltage and high-power device applications.

ACKNOWLEDGMENTS

This work is supported by the National Key Science & Technology Special Project (Grant No. 2011ZX01002), the Major Program and State Key Program of National Natural Science Foundation of China (Grant No. 60890191), and the National Key Basic Research Program of China (973 Program).

[1]T. P. Chow and R. Tyagi, IEEE Trans. Electron Devices **41**, 1481 (1994).
[2]W. Saito, Y. Takada, M. Kuraguchi, K. Tsuda, I. Omura, T. Ogura, and H. Ohashi, IEEE Trans. Electron Devices **50**, 2528 (2003).
[3]J. S. Xue, Y. Hao, X. W. Zhou, J. C. Zhang, C. K. Yang, X. X. Ou, L. Y. Shi, H. Wang, L. A. Yang, and J. F. Zhang, J. Cryst. Growth **314**, 359 (2011).
[4]W. Saito, T. Domon, I. Omura, M. Kuraguchi, Y. Takada, K. Tsuda, and M. Yamaguchi, IEEE Electron Device Lett. **27**, 326 (2006).
[5]E. Bahat-Treidel, O. Hilt, F. Brunner, V. Sidorov, J. Würfl, and G. Tränkle, IEEE Trans. Electron Devices **57**, 1208 (2010).
[6]L. Wang, W. D. Hu, X. S. Chen, and W. Lu, J. Appl. Phys. **108**, 054501 (2010).
[7]L. Wang, X. S. Chen, W. D. Hu, J. Wang, J. Wang, X. D. Wang, and W. Lu, Appl. Phys. Lett. **99**, 063502 (2011).
[8]L. Wang, W. Hu, J. Wang, X. Wang, S. Wang, X. Chen, and W. Lu, Appl. Phys. Lett. **100**, 123501 (2012).
[9]R. Chu, Y. Zhou, J. Liu, D. Wang, K. J. Chen, and K. M. Lau, IEEE Trans. Electron Devices **52**, 438 (2005).
[10]S. Zhang, M. C. Li, Z. H. Feng, B. Liu, J. Y. Yin, and L. C. Zhao, Appl. Phys. Lett. **95**, 212101 (2009).
[11]J. S. Xue, J. C. Zhang, Y. W. Hou, H. Zhou, J. F. Zhang, and Y. Hao, Appl. Phys. Lett. **100**, 013507 (2012).
[12]J. Liu, Y. Zhou, R. Chu, Y. Cai, K. J. Chen, and K. M. Lau, IEEE Electron Device Lett. **26**, 145 (2005).
[13]C. X. Wang, K. Tsubaki, N. Kobayashi, T. Makimoto, and N. Maeda, Appl. Phys. Lett. **84**, 2313 (2004).
[14]J. Liu, Y. Zhou, J. Zhu, K. M. Lau, and K. J. Chen, IEEE Electron Device Lett. **27**, 10 (2006).
[15]J. Ma, J. Zhang, J. Xue, Z. Lin, Z. Liu, X. Xue, X. Ma, and Y. Hao, J. Semicond. **33**, 014002 (2012).
[16]E. Bahat-Treidel, O. Hilt, F. Brunner, J. Würfl, and G. Tränkle, Phys. Status Solidi C **6**, 1373 (2009).
[17]D. Visalli, M. V. Hove, J. Derluyn, S. Degroote, M. Leys, K. Cheng, M. Germain, and G. Borghs, Jpn. J. Appl. Phys. **48**, 04C101 (2009).
[18]L. Shen, S. Heikman, B. Moran, R. Coffie, N. Q. Zhang, D. Buttari, I. P. Smorchkova, S. Keller, S. P. DenBaars, and U. K. Mishra, IEEE Electron Device Lett. **22**, 457 (2001).
[19]N. Maeda, K. Tsubaki, T. Saitoh, and N. Kobayashi, Appl. Phys. Lett. **79**, 1634 (2001).
[20]M. J. Wang, B. Shen, F. J. Xu, Y. Wang, J. Xu, S. Huang, Z. J. Yang, K. Xu, and G. Y. Zhang, Appl. Phys. A **88**, 715 (2007).
[21]M. A. Moram and M. E. Vickers, Rep. Prog. Phys. **72**, 036502 (2009).
[22]T. Zywietz, J. Neugebauer, and M. Scheffler, Appl. Phys. Lett. **73**, 487 (1998).
[23]V. Lebedev, K. Tonisch, F. Niebelschütz, V. Cimalla, D. Cengher, I. Cimalla, Ch. Mauder, S. Hauguth, O. Ambacher, F. M. Morales, J. G. Lozano, and D. González, J. Appl. Phys. **101**, 054906 (2007).
[24]W. Liu and A. A. Balandin, J. Appl. Phys. **97**, 073710 (2005).
[25]D. Zanato, S. Gokden, N. Balkan, B. K. Ridley, and W. J. Schaff, Semicond. Sci. Technol. **19**, 427 (2004).
[26]A. Asgari, S. Babanejad, and L. Faraone, J. Appl. Phys. **110**, 113713 (2011).
[27]S. B. Lisesivdin, S. Acar, M. Kasap, S. Ozcelik, S. Gokden, and E. Ozbay, Semicond. Sci. Technol. **22**, 543 (2007).
[28]M. J. Kearney and A. I. Horrell, Semicond. Sci. Technol. **13**, 174 (1998).
[29]B. K. Ridley, J. Phys. C: Solid State Phys. **15**, 5899 (1982).
[30]D. C. Look and R. J. Molnar, Appl. Phys. Lett. **70**, 3377 (1997).